

# ComplexBeat: Breathing Rate Estimation from Complex CSI

Sitian Li\*, Andreas Toftegaard Kristensen\*, Andreas Burg\*, Alexios Balatsoukas-Stimming†

\*Telecommunication Circuits Laboratory, École polytechnique fédérale de Lausanne, Switzerland

†Eindhoven University of Technology, the Netherlands

**Abstract**—In this paper, we explore the use of channel state information (CSI) from a WiFi system to estimate the breathing rate of a person in a room. In order to extract WiFi CSI components that are sensitive to breathing, we propose to consider the delay domain channel impulse response (CIR), while most state-of-the-art methods consider its frequency domain representation. One obstacle while processing the CSI data is that its amplitude and phase are highly distorted by measurement uncertainties. We thus also propose an amplitude calibration method and a phase offset calibration method for CSI measured in orthogonal frequency-division multiplexing (OFDM) multiple-input multiple-output (MIMO) systems. Finally, we implement a complete breathing rate estimation system in order to showcase the effectiveness of our proposed calibration and CSI extraction methods.

**Index Terms**—Vital signs monitoring, Channel state information, WiFi OFDM sensing, OFDM phase calibration, OFDM amplitude calibration.

## I. INTRODUCTION

The observation of vital signs is an essential part of health monitoring, both for hospitalized patients and healthy people in daily life. Breathing rate, for instance, is an early and extremely good indicator of physiological conditions such as hypoxia (low levels of oxygen in the cells) and hypercapnia (high levels of carbon dioxide in the bloodstream) [1]. A polysomnograph (PSG) is a device designed for sleep studies, which consists of belts around the chest and upper abdominal wall for monitoring the body movements from breathing [2]. Compared to such intrusive or attached devices, non-contact radio frequency (RF) sensors can observe vital signs using the fact that RF signal transmission is influenced by small changes in the environment, without introducing discomfort to users.

Initial systems for wireless health monitoring were based on radar, which sends pulses that are reflected and estimates the round-trip time which corresponds to the distance between the sensor and the human body for monitoring the human chest movement during breathing [3, 4]. To deal with multipath channels, frequency modulated carrier wave (FMCW) radars were employed by [5, 6].

Relying on WiFi is another, often more convenient, solution for wireless sensing of vital signs since WiFi transceivers are already widely deployed. Commercial WiFi employs orthogonal frequency-division multiplexing (OFDM) for signal transmission, which decomposes the channel into multiple subcarriers. By sending pilots, the

channel impulse response (CIR) can be measured, which provides magnitude and phase information of the different signal propagation paths. Existing vital signs sensing methods consider the frequency domain representation of the CIR to estimate the chest displacement as in [7]. This representation, composed of multiple subcarriers, is readily available in OFDM systems and is typically referred to as channel state information (CSI) in the corresponding computer science literature.

The survey in [8] lists a wide range of works on sensing with WiFi. Recent works on breathing rate estimation based on OFDM WiFi can be broadly grouped into two categories. In the first category, the breathing rate is estimated by observing periodic CSI amplitude changes in subcarriers [7, 9, 10, 11]. In the second category, the phase of the CSI is used for breathing rate estimation. The work in [12], nick-named PhaseBeat, introduced a method to estimate breathing rate information from the phase difference between two antennas of a multiple-input multiple-output (MIMO) WiFi device with multiple antenna pairs. Moreover, FullBreathe [13] and ResBeat [14] estimate breathing rate based on both CSI amplitude and phase, where one component is complementary to the other, depending on the position of the person. However, these methods treat the CSI amplitude and phase separately as two independent, real-valued measurements, where the complex-valued nature of the CSI is ignored. Yet, considering the amplitude and phase as a single complex-valued measurement is more natural as treating them independently: On the one hand, the inverse discrete Fourier transform (IDFT) of the complex-valued CSI is the CIR, in which only the bin with a certain delay, depending on the position of the person, is relevant to the breathing movement. This component can then be isolated. On the other hand, since both amplitude and phase of the CSI contain the information of breathing rate, it is easier to directly observe the periodicity in the complex-valued CSI stream.

Unfortunately, each CSI snapshot is affected by a different amplitude distortion caused by the automatic gain control (AGC) [15] and a different phase distortion caused by offsets such as sampling frequency offset (SFO), carrier frequency offset (CFO), and packet boundary detection (PBD) error [8]. Therefore, a good amplitude and phase calibration for removing measurement artifacts is necessary for estimating the breathing rate from the CSI. The works in [7, 10] employ low-pass filters on the CSI amplitude along time to reduce the influence of AGC. In [16], the AGC is eliminated by scaling the CSI amplitude

by the sum of CSI amplitude squared over all subcarriers. To cancel the influence of phase offsets, the works of [12, 14] employ a receiver with multiple antennas and use the phase of one of the antennas as a reference to be subtracted from other antennas. Another method is to use the linear component in the phase with respect to subcarrier indices as a reference to eliminate phase distortion [17].

### Contributions

In this paper, we introduce a novel CSI calibration method for both amplitude and phase distortions. We calibrate the amplitude of the CSI based on the amplitude of the dominant path in the CIR. The phase is calibrated by the linear components of the CSI phase of the adjacent receiver antenna. Both the complex-valued CSI and CIR are then used to estimate the breathing rate, after carefully selecting the most relevant signal components. We implement two different breathing rate estimation systems with tunable parameters and test them on the same publicly available data set [18], to evaluate our proposed calibration and extraction methods.

## II. PRELIMINARIES

In this section, we describe the structure of the CSI and the CSI phase distortion. Moreover, we explain the phase difference method described in [12] as basis for the proposed improvements described in Section III. Finally, we discuss the existing subcarrier selection and periodicity detection methods for breathing rate estimation using CSI data.

### A. CSI in WiFi MIMO OFDM Systems

Consider an OFDM system operating over a multipath channel. The transmitter sends training information and the receiver extracts the complex baseband CSI that can be described as

$$H_m = \sum_{p=1}^P A_p e^{-j2\pi(\Delta f m + f_c)\tau_p}, \quad (1)$$

where  $P$  is the number of paths,  $A_p$  and  $\tau_p$  are the attenuation and delay of path  $p$ , respectively,  $m$  is the subcarrier index,  $\Delta f$  is the subcarrier spacing and  $f_c$  is the carrier frequency. Note that  $\Delta f m$  is the baseband carrier frequency, which is between  $-\frac{B}{2}$  and  $\frac{B}{2}$ , where  $B$  is the bandwidth. In an OFDM communication system, the CSI has  $M$  entries, and each entry is a function of  $\tau_p$ , which can be used to estimate the change of  $\tau_p$  over time.

For the WiFi MIMO OFDM case, where there is more than one transmitter (TX) / receiver (RX) antenna pair, the CSI can be written as a tensor  $H_{i,j,m} \in \mathbb{C}^{N_T \times N_R \times M}$ , where  $N_T$  and  $N_R$  are the number of TX and RX antennas, respectively. To observe the change in the channel, multiple CSI snapshots are obtained. A CSI sample set is written as a four-dimensional tensor  $H_{i,j,m}[t] \in \mathbb{C}^{T \times N_T \times N_R \times M}$ , where  $T$  is the number of snapshots.

### B. CSI Phase Distortion and RX Phase Difference

When transmitter and receiver are not synchronized and phase noise is present, PBD error, SFO, and CFO have an

influence on the phase of the CSI. The phase of the CSI sample set, including these distortions can be described as [19, 20, 21]

$$\angle \tilde{H}_{i,j,m}[t] = \angle H_{i,j,m}[t] + (\xi_i^d[t] + \xi_i^s[t])m + \xi_i^c[t] + \gamma_i[t], \quad (2)$$

where  $\angle \tilde{H}_{i,j,m}[t]$  is the distorted CSI phase value for TX antenna  $i$ , RX antenna  $j$  and subcarrier index  $m$  at snapshot  $t$ . The variable  $\gamma_i$  is the initial phase offset due to the phase-locked loop (PLL),  $\xi_i^d$ ,  $\xi_i^s$ , and  $\xi_i^c$  are the phase errors from the PBD error, SFO, and CFO, respectively for TX antenna  $i$  [19, 20, 21]. The offset values are identical for all RX antennas on the same receiver at the same snapshot  $t$ . In order to eliminate the unknown phase component  $(\xi_i^d[t] + \xi_i^s[t])m + \xi_i^c[t] + \gamma_i[t]$ , the work of [12] proposed to subtract  $\angle \tilde{H}_{i,j',m}[t]$  from  $\angle \tilde{H}_{i,j,m}[t]$ , where  $j' \neq j$ , and obtain the RX phase difference  $\angle H_{i,k,m}[t]$

$$\angle \tilde{H}_{i,k,m}[t] = \angle H_{i,j,m}[t] - \angle H_{i,j',m}[t]. \quad (3)$$

According to [12, Lemma 1], when the wireless signal is reflected from the chest of a person with a breathing frequency  $f_r$ , the true phase of the reflected signal at any antenna of the receiver is also periodic with the same frequency  $f_r$ . The phase difference  $\angle \tilde{H}_{i,k,m}[t]$ , as the linear combination of  $\angle H_{i,j,m}[t]$  and  $\angle H_{i,j',m}[t]$ , contains this periodic component of  $f_r$  as well. However, the drawback of this calibration is that the resulting CSI with (3) as its phase component no longer reflects the physical CIR.

### C. Signal Component Selection

Even though it has been shown that the phase of the CSI is periodic with  $f_r$ , several works [12, 13, 14] have shown that the phase component of different subcarriers shows different sensitivity to breathing movement. To select a suitable subcarrier, a mean absolute deviation (MAD)-based method is proposed in [12] in which three subcarriers with the largest maximum MAD on measured phase difference are pre-selected. Then the subcarrier with the median MAD value among the pre-selected three candidates is finally selected.

Another possible selection method is based on band-of-interest (BoI) analysis. The corresponding selection criterion is based on the power spectral density (PSD)  $P_{i,j,m}[f]$  along the snapshot axis of any measured and calibrated quantity, which can be either the phase difference of the CSI or the complex-valued CSI or CIR directly. From the PSD, a score  $S$  is obtained as

$$S_{i,j,m} = \frac{\sum_{f_r^l \leq |f| \leq f_r^h} |P_{i,j,m}[f]|^2}{\sum_{|f| > f_r^h} |P_{i,j,m}[f]|^2}, \quad (4)$$

where  $f_r^l$  and  $f_r^h$  are the lower and upper limits of the human breathing rate  $f_r$ . The band between  $f_r^l$  and  $f_r^h$  is the BoI. The larger  $S_{i,j,m}$  is, the more likely it is that the snapshot sequence with  $i$ ,  $j$  and  $m$  is sensitive to breathing movement.

### D. Breathing Rate Estimation

After selecting the best candidate, denoted with indices  $i^*$ ,  $j^*$  and  $m^*$ , we detect the breathing rate from the signal component (e.g.,  $\tilde{H}_{i^*,j^*,m^*}[t]$ ) along snapshots  $t$ . In the work of [7] and [12], a peak detection method is used to extract

breathing rate information. The local peaks along  $t$  are first detected, and fake peaks are removed using [7, Algorithm 1]. After peak detection, all peak-to-peak intervals are averaged to obtain the periodicity of the breathing signal [12].

However, our analysis shows that this peak detection is not robust against noise in the signal change along time. Once there is one peak suppressed by noise or interference, there will be a large error in the breathing rate estimation. Thus, we also consider the PSD-detect method described in [10]. Specifically, we compute the PSD of the selected signal component with higher resolution by padding zeros to the end of the measurement (along the time axis). The frequency at which the PSD is maximum is returned as the estimated breathing rate. This PSD-detect method can also be applied to the complex-valued waveform over  $t$ .

### III. COMPLEXBEAT

In this section, we first introduce a new CSI calibration method that preserves most of the ground truth phase information in the original, uncalibrated CSI. Then we further process the calibrated complex CSI in the delay domain. The uncalibrated CSI at snapshot  $t$  is the ground truth CSI multiplied by an AGC term  $A_j^{\text{AGC}}$  [15, 22] and a phase offset term [19, 20, 21]

$$\tilde{H}_{i,j,m}[t] = A_j^{\text{AGC}}[t] H_{i,j,m}[t] e^{j2\pi((\xi_i^d[t] + \xi_i^s[t])m + \xi_i^c[t] + \gamma_i[t])}. \quad (5)$$

#### A. CSI Amplitude Calibration: Dominant Path Approach

In order to cancel the amplitude distortion caused by the AGC, we introduce an amplitude calibration based on the dominant component in the CIR. Since the  $A_j^{\text{AGC}}[t]$  is the same for each subcarrier  $m$ , the distorted amplitude of the measured CIR is  $|\tilde{h}_{i,j,\tau}[t]| = A_j^{\text{AGC}}[t] |h_{i,j,\tau}[t]|$ . Now we assume that (i) the delay spread is small, i.e., that there is a dominant path between the transmitter and the receiver, (ii) the path reflected on the human chest is the only dynamic path, and (iii) that the breathing movement has very little impact on the amplitude of the dominant path in the CIR. We first determine the dominant path by finding  $\tau_{i,j,t}^* = \arg \max_{\tau} |\tilde{h}_{i,j,\tau}[t]|$ . Then we calculate the calibrated CSI as

$$\begin{aligned} |\hat{H}_{i,j,m}[t]| &= \left( \frac{1}{2D+1} \sqrt{\sum_{|\tau - \tau_{i,j,t}^*| \leq D} |\tilde{h}_{i,j,\tau}[t]|^2} \right)^{-1} |\tilde{H}_{i,j,m}[t]| \\ &= \left( \frac{1}{2D+1} \sqrt{\sum_{|\tau - \tau_{i,j,t}^*| \leq D} |h_{i,j,\tau}[t]|^2} \right)^{-1} |H_{i,j,m}[t]|, \end{aligned} \quad (6)$$

with a small  $D$  that is selected such that the term,  $\sum_{|\tau - \tau_{i,j,t}^*| \leq D} |h_{i,j,\tau}[t]|^2$  covers the power in the dominant path. With the assumption that the breathing movement has very little impact on the amplitude of the dominant path and that the other paths in the environment are stable, the calibrated CSI amplitude  $|\hat{H}_{i,j,m}[t]|$  is the ground truth CSI amplitude  $|H_{i,j,m}[t]|$  multiplied by an almost constant term that is not changing over time  $t$ .

#### B. CSI Phase Calibration: Linear Component Approach

Instead of calculating the difference between the phase components on two RX antennas as shown in [12], we introduce a calibration method that preserves most of the phase information of the CSI. To this end, we exploit that the phase offsets, as shown in (2), for all RX antennas are identical and are linear functions of the subcarrier index  $m$ . We thus write the term  $(\xi_i^d[t] + \xi_i^s[t])m + \xi_i^c[t] + \gamma_i[t]$  as  $\alpha_i^{\text{off}}[t]m + \beta_i^{\text{off}}[t]$ , which yields

$$\angle \tilde{H}_{i,j,m}[t] = \angle H_{i,j,m}[t] + (\alpha_i^{\text{off}}[t]m + \beta_i^{\text{off}}[t]). \quad (7)$$

As in Section III-A, we assume that the delay spread is small, and that the path reflected on the human chest is the only dynamic path. Then, the CSI phase  $\angle H_{i,j,m'}[t]$  of a small subset of adjacent subcarriers  $m'$  can also be approximated as linear with respect to  $m'$  and the corresponding linear coefficients are denoted as  $\alpha'_{i,j}[t]$  and  $\beta'_{i,j}[t]$ . With the influence of phase distortion, the linear trend coefficients along  $m'$  of  $\angle \tilde{H}_{i,j,m'}[t]$  become  $\tilde{\alpha}'_{i,j}[t] = \alpha'_{i,j}[t] + \alpha_i^{\text{off}}[t]$  and  $\tilde{\beta}'_{i,j}[t] = \beta'_{i,j}[t] + \beta_i^{\text{off}}[t]$ , where  $\tilde{\alpha}'_{i,j}[t]$  and  $\tilde{\beta}'_{i,j}[t]$  can be obtained from the CSI phase measurement  $\angle \tilde{H}_{i,j,m}[t]$ . We then calibrate the CSI phase on the RX antenna with index  $j+1$  by subtracting  $\tilde{\alpha}'_{i,j}[t]m + \tilde{\beta}'_{i,j}[t]$  from it. Note that the RX antenna index computation must be performed modulo  $N_R$ . After calibration, the CSI is written as

$$\angle \hat{H}_{i,j+1,m}[t] = \angle H_{i,j+1,m}[t] - (\alpha'_{i,j}[t]m + \beta'_{i,j}[t]). \quad (8)$$

If the signal reflected on the human chest is not on the dominant path for both antennas and the dominant path is static over time, the calibrated  $\angle \hat{H}_{i,j+1,m}$  is the true CSI phase for antenna  $j+1$  plus a term,  $-j(\alpha'_{i,j}[t]m + \beta'_{i,j}[t])$  that is almost constant across snapshots  $t$  for all  $m$ , as shown in (8). However, if the signal reflected on the human chest is on the dominant path, i.e., the breathing movement affects  $\alpha'_{i,j}[t]$  and  $\beta'_{i,j}[t]$ , the phase of (8) still contains the term  $(\alpha'_{i,j+1}[t] - \alpha'_{i,j}[t])m + (\beta'_{i,j+1}[t] - \beta'_{i,j}[t])$ , which still has a periodic component of  $f_r$ , according to [12, Lemma 1]. In this case, our method has an advantage compared to the similar self-linear calibration method discussed in [17], where the antenna is calibrated by its own linear phase component which causes the phase term that contains useful breathing rate information to vanish.

#### C. Delay Domain Detection and Filter

Since the amplitude and the phase distortion of the CSI are eliminated by the calibration while preserving most of the phase information, we can transform the CSI  $H_{i,j,m}[t]$  into the delay domain as CIR  $\hat{h}_{i,j,\tau}[t]$ . From the CIR, we find the delay component  $\tau^*$ , that contains the maximum signal power in the BoI.

However, the delay resolution of the CIR is very low due to the narrow bandwidth in OFDM WiFi. The breathing component may therefore be spread across multiple bins in the CIR. In order to combine the information in multiple selected bins in the CIR, we preserve all potentially relevant bins and transform the CIR back into CSI representation. We then select the one most relevant (e.g., according to the BoI criterion) CSI component instead of a single CIR component, since all

entries of the CSI are a linear combination of the CIR bins. We refer to the selection of a range of bins in the CIR as delay filter (DF). A straight forward approach to determine a range of taps to preserve is based on an upper bound  $\tau_{\max}$  for the delay of relevant single-reflection paths on the human chest. All CIR components with a delay  $|\tau| > \tau_{\max}$  are set to zero and the resulting filtered CIR is transformed back into the frequency domain  $\hat{H}'_{i,j,m}[t]$ ,

$$\hat{H}'_{i,j,m}[t] = \mathcal{F}_{\tau \rightarrow m} \left( \begin{cases} \mathcal{F}_{m \rightarrow \tau}^{-1}(\hat{H}_{i,j,m}[t]), & \text{if } |\tau| \leq \tau_{\max} \\ 0, & \text{otherwise} \end{cases} \right). \quad (9)$$

#### IV. SYSTEM STRUCTURE

In this section, we describe two different breathing rate estimation systems, PhaseBeat [12] and our proposed ComplexBeat system, each with different variants. All systems start from a set of CSI parameter estimates  $\tilde{H}_{i,j,m}[t] \in \mathbb{C}^{T \times N_T \times N_R \times M}$ . The corresponding data flows are shown in Fig. 1a for PhaseBeat and in Fig. 1b for ComplexBeat. Both systems have blocks whose function can be configured.

In the PhaseBeat setup, the candidate selection block and the rate detection block can be configured with different methods. By configuring the methods for each block, we obtain the PhaseBeat system as in [12] and its two variants:

- 1) The PhaseBeat system, which employs the phase difference method and uses the MAD-based candidate selection method and peak detection method as proposed in [12].
- 2) PhaseBeat-MAD-PSD, which augments PhaseBeat with PSD-based rate detection method.
- 3) PhaseBeat-BoI-PSD, which replaces the MAD-based selection in PhaseBeat-MAD-PSD with the BoI selection method.

In ComplexBeat, after implementing our calibration method, we can use either the CIR or CSI data representation for further processing. If the CSI is used, an optional delay filter is applied. Different configurations also lead to three ComplexBeat setups for performance comparison:

- 1) ComplexBeat-CIR, which implements our calibration method and then applies CIR for breathing rate estimation, with BoI selection and PSD rate detection.
- 2) ComplexBeat-CSI, which modifies ComplexBeat-CIR by using CSI for breathing rate estimation. The delay filter is turned off.
- 3) ComplexBeat-CSI-DF, which augments ComplexBeat-CSI by activating the delay filter.

##### A. PhaseBeat

PhaseBeat [12] first calculates the CSI phase difference between two adjacent RX antennas  $j$  and  $j' \neq j$  as shown in (3).

After extracting the CSI phase difference  $\angle \tilde{H}_{i,k,m}$  for  $i \in [0, N_T - 1]$  and  $k \in [0, (N_R - 1) - 1]$ , the algorithm determines

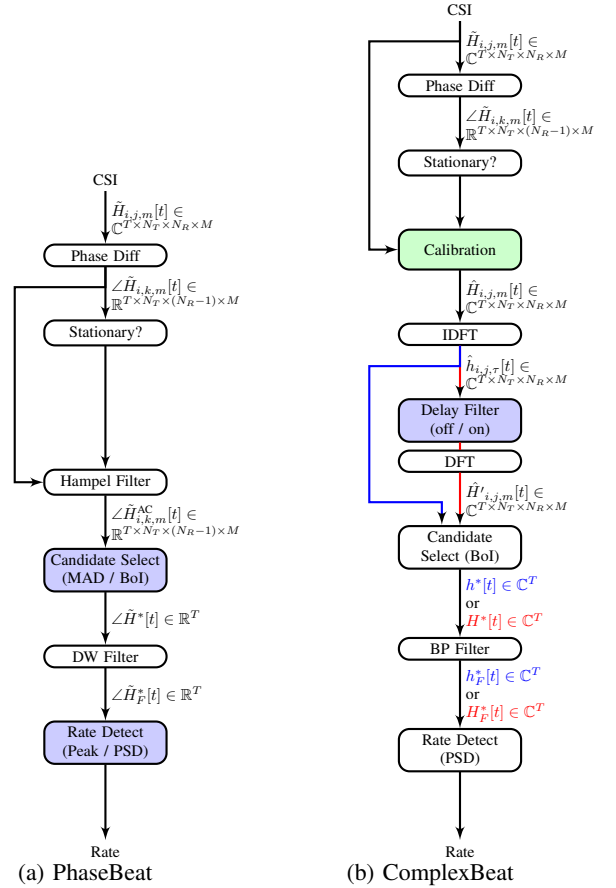


Fig. 1: System Structures

whether the person is in a stationary state based on a score

$$Q = \frac{1}{N_T \cdot (N_R - 1) \cdot M \cdot T} \times \sum_i \sum_k \sum_m \sum_{t=0}^{T-1} |\angle \tilde{H}_{i,k,m}[t] - \mathbb{E}_t[\angle \tilde{H}_{i,k,m}[t]]|. \quad (10)$$

Breathing rate estimation is only performed on sample sets for which  $Q < 0.18$ , since only these are considered as sufficiently stable.

For each stable sample set, we apply a Hampel filter with a window size of 5 seconds and a threshold of 0.01 to filter out the DC component as proposed in [12]. The DC component is subtracted from  $\angle \tilde{H}_{i,k,m}[t]$ , which leads to a detrended waveform  $\angle \tilde{H}_{i,k,m}^{AC}[t]$ . Then a selection of the most sensitive candidate subcarriers is performed. PhaseBeat and PhaseBeat-MAD-PSD use the MAD-based selection method, whereas the PhaseBeat-BoI-PSD applies the BoI-based method with  $f_r^h = 0.5$  Hz and  $f_r^l = 0.2$  Hz.

The selected candidate is then a 1D signal as a function of  $t$ , denoted as  $\angle \tilde{H}^*[t]$ . A discrete wavelet (DW) filter is then applied to  $\angle \tilde{H}^*[t]$ . We calculate the “db4” Daubechies

decomposition to  $\angle \tilde{H}^*[t]$  as in [12],

$$\begin{aligned} \angle \tilde{H}^*[t] &= \sum_{k \in \mathbb{Z}} \lambda^{(L)}[k] \phi^{(L)}[t - 2^L k] \\ &+ \sum_{l=1}^L \sum_{k \in \mathbb{Z}} \mu^{(l)}[k] \psi^{(l)}[t - 2^l k]. \end{aligned} \quad (11)$$

We then only keep the wavelet components whose frequencies are in the range of human breathing rates (from 0 to 0.5 Hz), which is the first term in (11). The value of  $L$  is determined based on the snapshot sampling frequency  $f_s$ , such that  $\frac{f_s}{2^{L+2}} < 0.5 \text{ Hz} \leq \frac{f_s}{2^{L+1}}$ . The coefficients  $\lambda^{(L)}[k]$  are calculated as  $\lambda^{(L)}[k] = \sum_{t \in \mathbb{Z}} \angle \tilde{H}^*[t] \phi^{(L)}[t - 2^L k]$ , where  $\phi^{(L)}[t]$  is the Daubechies wavelet on level  $L$ .

In the end, we calculate the breathing rate using both the peak-detect and the PSD-detect methods as discussed in Section II-D. PhaseBeat uses the peak-detect method. PhaseBeat-MAD-PSD and PhaseBeat-BoI-PSD apply the PSD-detect method with a resolution of 0.001 Hz. The frequency between 0.2 Hz and 0.5 Hz for which the PSD is maximized is chosen as the breathing rate estimate  $f_r$ .

### B. ComplexBeat

In this setup, we employ our proposed CSI calibration as discussed in Section III-A and Section III-B, for each sample set that is deemed stable according to (10), using (6) and (8). Due to frequency selective fading, we select the subcarriers  $m'$  whose amplitude is large to extract  $\tilde{\alpha}'_{i,j}[t]$  and  $\tilde{\beta}'_{i,j}[t]$ , and calibrate  $\angle \tilde{H}_{i,j+1,m}[t]$  with  $-(\tilde{\alpha}'_{i,j}[t]m + \tilde{\beta}'_{i,j}[t])$ . We can continue processing the calibrated data either in its CIR form (ComplexBeat-CIR, blue thread in Fig. 1b) or in its CSI form (ComplexBeat-CSI and ComplexBeat-CSI-DF, red thread in Fig. 1b).

ComplexBeat-CIR first obtains the CIR and then uses the BoI selection method with  $f_r^h = 0.5 \text{ Hz}$  and  $f_r^l = 0.2 \text{ Hz}$ , based on the PSD of  $\hat{h}_{i,j,\tau}[t]$  to determine  $i^*$ ,  $j^*$ , and  $\tau^*$  as discussed in Section II-C. We then use the CIR component  $h^*[t] = \hat{h}_{i^*,j^*,\tau^*}[t]$  for further processing. Both ComplexBeat-CSI and ComplexBeat-CSI-DF operate on the complex-valued CSI. In ComplexBeat-CSI-DF, we apply the delay domain filter with  $\tau_{\max} = 50 \text{ ns}$  to the complex-valued CSI, as shown in (9) in Section III-C. If the delay filter is off, as configured in ComplexBeat-CSI, the input CSI is directly copied to the output such that  $\hat{H}'_{i,j,m}[t] = \hat{H}_{i,j,m}[t]$ . For both ComplexBeat-CSI and ComplexBeat-CSI-DF, the CSI candidate with the highest score  $H^*[t] = \hat{H}'_{i^*,j^*,m^*}[t]$  in the BoI selection is used for further processing.

For all three variants, a band-pass filter is then applied by first transforming the complex series  $H^*[t]$  or  $h^*[t]$  into their spectrum  $P^*[f]$ , and setting the values on  $|f| < 0.2 \text{ Hz}$  and  $|f| > 0.5 \text{ Hz}$  to zero, and then transforming it back to time domain  $H_F^*[t]$  or  $h_F^*[t]$ . In the end, the PSD-detection method same as in Section IV-A is employed for breathing rate detection.

## V. EXPERIMENTAL STUDY

In this section, we evaluate the accuracy of the two systems and their variants that are described in Section IV on the same data set.

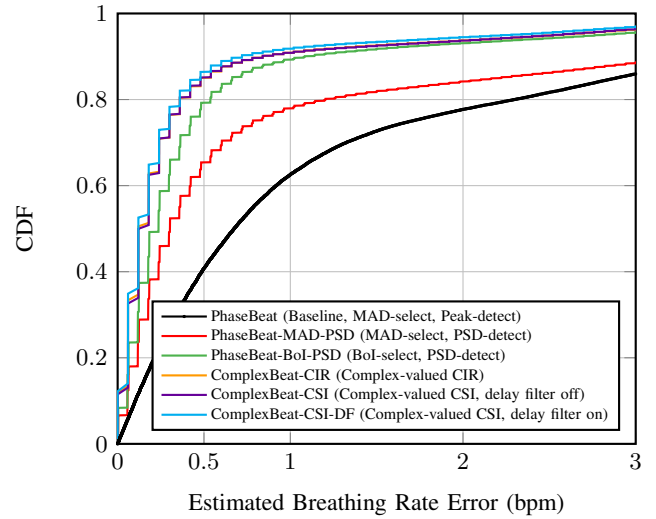


Fig. 2: CDF of estimation error with breathing rate range from 0.2 to 0.3 Hz, where the CDF of ComplexBeat-CIR (—) is almost covered by the CDF of ComplexBeat-CSI (—).

### A. Data Set

We use the data set provided with [18]. This data set records the CSI from a WiFi MIMO OFDM system that is running overnight, while patients are sleeping between the transmitter and the receiver. The WiFi system consists of two TX antennas and two RX antennas and operates in the 5 GHz ISM band with 114 subcarriers in a 40 MHz bandwidth. To make the dataset structure as similar as possible to the dataset used in [12], where there are one TX and two RX antennas operating in a bandwidth of 20 MHz with 30 subcarriers, we only keep the measured data on one TX antenna and the upper half frequency band. We pick every second subcarrier, which yields 29 subcarriers. CSI data is sampled for each antenna pair at a sampling rate of 9.9 Hz. By sliding a window with a size of 30 seconds, we obtain the CSI  $H_{i,j,m}[t] \in \mathbb{C}^{297 \times 1 \times 2 \times 29}$ . For each new estimation iteration, we slide the time window by 1 second. To check the estimation performance for different ground truth breathing frequencies, we picked the patients with indices {00, 03, 06, 07, 10, 11, 12, 16}, for which PhaseBeat shows a good absolute estimation error below 1.2 beats per minute (bpm) for more than 60% of the considered snapshots. This set of patients' breathing rate covers the range from 0.2 to 0.5 Hz, i.e., 12 to 30 bpm.

The data set also offers PSG data as a reference, from which we obtain the ground truth breathing rate with the method described in [18].

### B. Performance Analysis and Comparison

Since the PhaseBeat system in [12] is only tested for breathing rate range from 0.2 to 0.3 Hz, we first compare the estimation error for the case where the ground truth breathing rate is within the range from 0.2 to 0.3 Hz. The CDFs of the absolute estimation errors are shown in Fig. 2. Two variants of PhaseBeat, PhaseBeat-MAD-PSD and PhaseBeat-BoI-PSD, show better performance than the original PhaseBeat. The

combination of the BoI-based selection method and the PSD-rate detection method shows the best performance, where 79% of the estimation error is less than 0.5 bpm. Our ComplexBeat system outperforms PhaseBeat and its variants. ComplexBeat-CIR and ComplexBeat-CSI achieve similar performance. With filtering in the delay domain, and the candidate selected in the frequency domain, ComplexBeat-CSI-DF shows the best result, where 86% of the estimation errors are below 0.5 bpm. We also calculated the CDF of the estimation error when the ground truth breathing rate is between 0.2 and 0.5 Hz. In this case, ComplexBeat-CSI-DF still shows the best performance among all the systems. Due to space limitations, the CDF plot for this case is not included in this paper.

## VI. CONCLUSIONS

In this paper, we show that robust breathing rate estimation from CSI relies on careful selection of the best CSI component, especially in the delay domain. To this end, we introduce a dominant path-based CSI amplitude calibration method and a linear component-based CSI phase calibration method for pre-processing of the CSI data. The calibration methods combined with the delay domain filtering leads to a better CSI extraction compared to PhaseBeat and its variants. Furthermore, we show that the breathing rate can be estimated directly from calibrated complex-valued CSI or CIR. Compared to observing only the phase values, the estimation from complex-valued CSI achieves the highest accuracy.

## ACKNOWLEDGMENT

This research has been kindly supported by the Swiss National Science Foundation under Grant-ID 182621.

## REFERENCES

- [1] S. Rolfe, "The importance of respiratory rate monitoring," *British Journal of Nursing*, vol. 28, no. 8, pp. 504–508, Apr. 2019.
- [2] S. R. Pandi-Perumal, D. W. Spence, and A. S. Bahammam, "Polysomnography: An overview," in *Primary Care Sleep Medicine*, J. F. Pagel and S. R. Pandi-Perumal, Eds. Springer New York, 2014, pp. 29–42.
- [3] S. Costanzo, "Software-defined Doppler radar sensor for human breathing detection," *Sensors*, vol. 19, no. 14, p. 3085, Jul. 2019.
- [4] A. Droitcour, O. Boric-Lubecke, and G. Kovacs, "Signal-to-Noise Ratio in Doppler radar system for heart and respiratory rate measurements," *IEEE Transactions on Microwave Theory and Techniques*, vol. 57, no. 10, pp. 2498–2507, Oct. 2009.
- [5] L. Anitori, A. de Jong, and F. Nennie, "FMCW radar for life-sign detection," in *2009 IEEE Radar Conference*. IEEE, 2009, pp. 1–6.
- [6] Z. Peng, J. M. Munoz-Ferreras, Y. Tang, C. Liu, R. Gomez-Garcia, L. Ran, and C. Li, "A portable FMCW interferometry radar with programmable Low-IF architecture for localization, ISAR imaging, and vital sign tracking," *IEEE Transactions on Microwave Theory and Techniques*, vol. 65, no. 4, pp. 1334–1344, Apr. 2017.
- [7] J. Liu, Y. Wang, Y. Chen, J. Yang, X. Chen, and J. Cheng, "Tracking vital signs during sleep leveraging off-the-shelf wifi," in *Proceedings of the 16th ACM International*

*Symposium on Mobile Ad Hoc Networking and Computing*, ser. MobiHoc '15. Association for Computing Machinery, 2015, p. 267–276.

- [8] Y. Ma, G. Zhou, and S. Wang, "WiFi sensing with channel state information: A survey," *ACM Computing Surveys*, vol. 52, no. 3, pp. 1–36, Jul. 2019.
- [9] S. Lee, Y.-D. Park, Y.-J. Suh, and S. Jeon, "Design and implementation of monitoring system for breathing and heart rate pattern using WiFi signals," in *2018 15th IEEE Annual Consumer Communications & Networking Conference (CCNC)*. IEEE, Jan. 2018, pp. 1–7.
- [10] P. Hillyard, A. Luong, A. S. Abrar, N. Patwari, K. Sundar, R. Farney, J. Burch, C. A. Porucznik, and S. H. Pollard, "Comparing respiratory monitoring performance of commercial wireless devices," *arXiv:1807.06767 [physics]*, Jul. 2018, arXiv: 1807.06767.
- [11] X. Liu, J. Cao, S. Tang, and J. Wen, "Wi-Sleep: Contactless sleep monitoring via WiFi signals," in *2014 IEEE Real-Time Systems Symposium*. IEEE, Dec. 2014, pp. 346–355.
- [12] X. Wang, C. Yang, and S. Mao, "PhaseBeat: Exploiting CSI phase data for vital sign monitoring with commodity WiFi devices," in *2017 IEEE 37th International Conference on Distributed Computing Systems (ICDCS)*. IEEE, Jun. 2017, pp. 1230–1239.
- [13] Y. Zeng, D. Wu, R. Gao, T. Gu, and D. Zhang, "Full-Breathe: Full human respiration detection exploiting complementarity of CSI phase and amplitude of WiFi signals," *Proceedings of the ACM on Interactive, Mobile, Wearable and Ubiquitous Technologies*, vol. 2, no. 3, pp. 1–19, Sep. 2018.
- [14] X. Wang, C. Yang, and S. Mao, "Resilient respiration rate monitoring with realtime bimodal CSI data," *IEEE Sensors Journal*, vol. 20, no. 17, pp. 10 187–10 198, Sep. 2020.
- [15] C. Chen, Y. Han, Y. Chen, H.-Q. Lai, F. Zhang, B. Wang, and K. J. R. Liu, "TR-Breath: Time-reversal breathing rate estimation and detection," *IEEE Transactions on Biomedical Engineering*, vol. 65, no. 3, pp. 489–501, 2018.
- [16] Z. Gao, Y. Gao, S. Wang, D. Li, and Y. Xu, "CRISLoc: Reconstructable CSI Fingerprinting for Indoor Smartphone Localization," *IEEE Internet of Things Journal*, vol. 8, no. 5, pp. 3422–3437, Mar. 2021. [Online]. Available: <https://ieeexplore.ieee.org/document/9187854/>
- [17] X. Wang, L. Gao, and S. Mao, "PhaseFi: Phase fingerprinting for indoor localization with a deep learning approach," in *2015 IEEE Global Communications Conference (GLOBECOM)*, 2015, pp. 1–6.
- [18] P. Hillyard, A. Luong, A. S. Abrar, N. Patwari, K. Sundar, R. Farney, J. Burch, C. Porucznik, and S. H. Pollard, "Experience: Cross-technology radio respiratory monitoring performance study," in *Proceedings of the 24th Annual International Conference on Mobile Computing and Networking*. ACM, Oct. 2018, pp. 487–496.
- [19] M. Speth, S. Fochtel, G. Fock, and H. Meyr, "Optimum receiver design for wireless broad-band systems

- using OFDM. I," *IEEE Transactions on Communications*, vol. 47, no. 11, pp. 1668–1677, Nov. 1999.
- [20] Y. Zhuo, H. Zhu, and H. Xue, "Identifying a New Non-Linear CSI Phase Measurement Error with Commodity WiFi Devices," in *2016 IEEE 22nd International Conference on Parallel and Distributed Systems (ICPADS)*. Wuhan, China: IEEE, Dec. 2016, pp. 72–79.
- [21] Y. Xie, Z. Li, and M. Li, "Precise power delay profiling with commodity Wi-Fi," *IEEE Transactions on Mobile Computing*, vol. 18, no. 6, pp. 1342–1355, Jun. 2019.
- [22] Y. Zhuo, H. Zhu, H. Xue, and S. Chang, "Perceiving accurate CSI phases with commodity WiFi devices," in *IEEE INFOCOM 2017 - IEEE Conference on Computer Communications*. IEEE, May 2017, pp. 1–9.